1 **Minería y Geología** / v.41 n.1/ january-march / 2025/ p. 1-16 ISSN 1993 8012

ORIGINAL ARTICLE

Petrographic Analysis of Ultramafic Rocks in a Zone of Cajálbana Massif, Western Cuba

Análisis petrográfico de las rocas ultramáficas de un sector del macizo Cajálbana, occidente de Cuba

Maria Elisabet Garcia-Crespo[1]*, Esther María Cruz-Gámez[1], Raydel Ramos-Pineda[1]

[1]University of Pinar del Río, Pinar del Río, Cuba.

*Corresnpondance´ Author: mariaelisabetgarciacrespo@gmail.com

Abstract

The Ultramafic Rocks of Cajálbana Massif (URCM) are part of the Northern Ophiolithic Belt (NOB) of Cuba. The massif outcrops as an irregular body in the western part of the island, Bahía Honda region in Pinar del Río province. The study presents the petrographic and geochemical analysis of 21 samples of peridotites and dunite from the SW sector of this massif and their comparison with similar lithology of the Belt. Results showed that during the magmatic process and after serpentinization RUMC, two fundamental stages of mineral formation occurred: one with olivine, pyroxenes (enstatite and augite) and Cr-spinel (stage 1), and another with lizardite, chrysotile, bastite, Fe3+-rich Cr-spinel and magnetite (stage 2). The Al_2O_3/SiO_2 ratios (0.02 - 0.06) and weight percent (wt %) of Al2O3 (1.17 - 2.43), TiO_2 (0.01 - 0.04) and CaO (0.04 - 2. 58) vary in these rocks, and are located within the range of ultramafic rocks of abyssal environment (portion of proto-Caribbean crust) and in overlapping zones of proto-Caribbean crust with the forearc (portion of Caribbean plate crust). Similar performance has been reported for the ultramafic rocks of the Villa Clara and Havana-Matanzas massifs.

Keywords: ophiolite, ultramafic rocks, serpentinization process, Cajálbana

Resumen

Las Rocas Ultramáficas del Macizo Cajálbana (RUMC) forman parte del Cinturón Ofiolítico Septentrional (COS) de Cuba. El macizo aflora en forma de un cuerpo irregular en la parte occidental de la isla, región de Bahía Honda (Pinar del Río). Aquí se presenta el análisis petrográfico y geoquímico de 21 muestras de peridotitas y dunitas del sector SW de este macizo, y su comparación con litologías similares del Cinturón. Los resultados revelaron que durante el proceso magmático y la posterior serpentinización de las RUMC ocurrieron dos etapas fundamentales de formación mineral: una con olivino, piroxenos (enstatita y augita) y Cr-espinela (etapa 1), y otra con lizardita, crisotilo, bastita, Cr-espinela rica en Fe^{3+} y magnetita (etapa 2). Las relaciones de Al_2O_3/SiO_2 (0.02 - 0.06) y el porcentaje en peso (wt%) de Al_2O_3 (1.17 - 2.43), TiO_2 (0.01 - 0.04) y CaO (0.04 - 2.58) varían en estas rocas, y se ubican dentro del rango de las rocas ultramáficas de ambiente abisal (porción de corteza proto-Caribe) y en zonas de solapamiento de la corteza proto-Caribe con el *forearc* (porción de corteza placa Caribe). Comportamiento similar se ha reportado para las rocas ultramáficas de los macizos Villa Clara y Habana- Matanzas.

Palabras claves: ofiolitas, rocas ultramáficas, serpentinización, Cajálbana

1. INTRODUCTION

Ophiolites are remnants of ancient oceanic crust and upper mantle that have been tectonically emplaced onto continental margins. According to Dilek and Furnes (2011), they can form in various settings: Continental Margins (CM), Mid-Ocean Ridges (MOR), Plumes (P), and Supra-Subduction Zones (SSZ). This study employs the English acronyms for these different settings.

Extensive outcrops of ophiolitic rocks are found in northern Cuba, constituting the so-called Northern Ophiolitic Belt (NOB; Iturralde-Vinent, 1990, 1996; Figure 1a). They typically exhibit the lithologies of an ideal ophiolite sequence, comprising serpentinized peridotite cumulates, a Moho Transition Zone (MTZ; sills and dikes), gabbroid rocks, diabase dikes, and basalts with sediments (Iturralde-Vinent, 1996). Significant chromite-spinel deposits are associated with these ophiolites, linked to the mantle tectonite levels and the MTZ. The age of these sequences ranges from 135 Ma to 60 Ma (Iturralde-Vinent, 1996; Proenza *et al*., 1999a, b; Marchesi *et al*., 2006; García-Casco *et al*., 2008a, 2008b).

The NOB represents a remnant of ancient lithosphere, possibly formed in MOR or SSZ settings. It comprises both MOR-type rocks unrelated to subduction (proto-Caribbean crust) and SSZ-type rocks related to subduction (Caribbean plate crust) (Iturralde-Vinent, 1996; Proenza *et al*., 1999a, 2006; García-Casco *et al*., 2003; Gervilla *et al*., 2005; Marchesi *et al*., 2006; Llanes-Castro *et al*., 2015; Butjosa *et al*., 2018, 2023).

The Moa-Baracoa and Mayarí-Cristal massifs represent two portions of a back-arc lithosphere. The Moa-Baracoa massif exhibits a geochemical signature similar to Mid-Ocean Ridge (MOR) settings, whereas the Mayarí-

Cristal massif shows an increasing role of H_2O in its petrogenesis and evidence of interaction with subduction-related magmas (Island Arc Tholeiite-IAT), indicating an original setting located closer to the paleo-volcanic arc than Moa-Baracoa (Marchesi *et al*., 2006).

Based on the composition of the ultramafic and mafic rocks from Villa Clara, Butjosa *et al*. (2018) classified them into two groups (A and B), revealing a complex, multi-stage formation of the oceanic lithosphere in diverse tectonic environments. Group A corresponds to fertile MORB-type mantle typical of abyssal/transform fault peridotites, while Group B exhibits characteristics of refractory fore-arc mantle wedge peridotites.

The Cajálbana massif is the westernmost ophiolitic unit in Cuban territory (Figure 1a) and one of the least studied in the country. It tapers northward, where it lies in tectonic contact beneath the allochthonous volcano-sedimentary sequence of the Cretaceous volcanic arc (represented by the Orozco Formation and its cover). To the south, the unit overlies the northern formations of the Guaniguanico range (Iturralde-Vinent, 1996).

The Ultramafic Rocks of the Cajálbana Massif (RUMC) constitute an allochthonous and sheared block within the remaining ophiolite sections (Figures 1b and 1c). Fonseca *et al*. (1984) indicate that the RUMC have a predominantly harzburgitic composition and, to a lesser extent, lherzolitic, dunitic, and pyroxenitic compositions, with varying degrees of serpentinization. Chromitite bodies within this massif are scarce, occurring as pods or slabs with thicknesses ranging from 5 cm to 25 cm. Based on chemical analysis, they are classified as metallurgical-grade chromites (Kravchenko and Vázquez, 1985).

Cruz-Gámez (1993) proposed an explanatory model for the development of the basalt layer in the Bahía Honda region and its relationship with sulfides, attributing a Back-Arc Basin (BAB) setting to this complex. More recently, Prieto *et al*. (2017) described the lithological characteristics of these rocks, particularly those outcropping in the southwestern extremity of the Cajálbana massif: harzburgite and, subordinately, dunite and orthopyroxenite, indicating that their crystallization occurred from a depleted lherzolitic mantle source.

This work presents a petrographic and geochemical analysis based on major oxides of the RUMC, aiming to reveal the petrological characteristics of these rocks and compare them with similar rocks from the Northern Ophiolitic Belt (NOB).

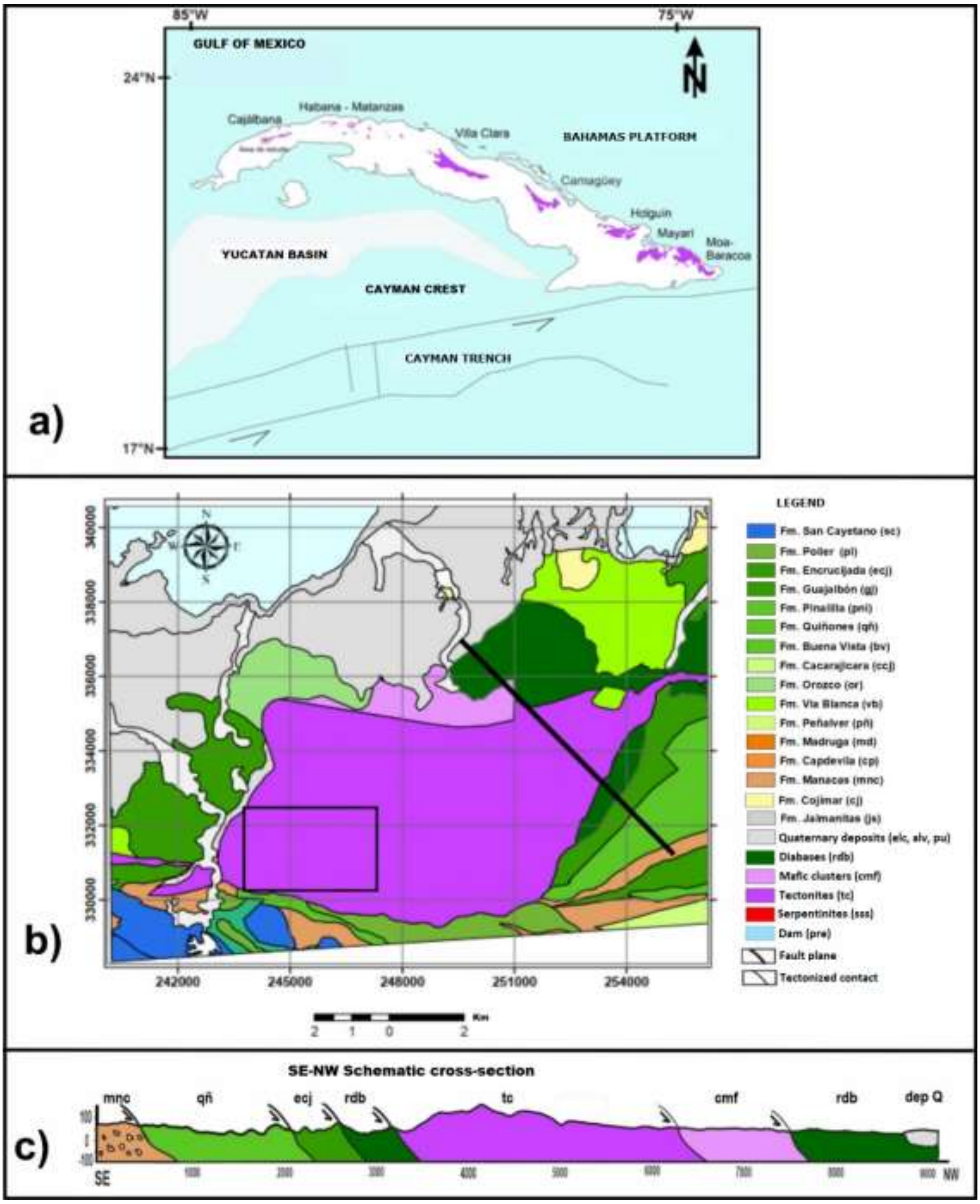

Figure 1. a) Main outcrops of the Northern Ophiolitic Belt (NOB) and regional geological framework. Modified from Iturralde-Vinent (1996) and Butjosa (2018). b) Geological sketch showing the relationship between the Ultramafic Rocks of the Cajálbana Massif (RUMC) and other geological units in the Bahía Honda zone (from the 1:100,000 scale geological map; IGP/SGC, 2010) and location of the study area. c) Geological profile illustrating the relationships of the RUMC with other ophiolitic rock sections, continental margin rocks, cover sequences, and recent sediments.

2. MATERIALS AND METHODS

Petrographic analysis was performed on a total of 21 samples of serpentinized peridotites collected from the southwestern part of the Cajálbana massif. The samples were studied using a standard Novel (NP-107 B) petrographic microscope at the University of Pinar del Río. For chemical analysis, the least weathered samples (13 samples) were selected. Major elements were analyzed at the Bureau Veritas Commodities Ltd. laboratory (Vancouver, Canada), obtained via the LF200 methodology. Each sample was fused using lithium borate, and the resulting melt was completely dissolved with hot aqua regia. Major elements were analyzed in the resulting solution by inductively coupled plasma optical emission spectrometry (ICP-OES detection limit for major elements: ~0.01%).

To contrast the results, they were compared with analyses reported by Marchesi *et al*. (2006) for samples from the Moa-Baracoa (n=16) and Mayarí-Cristal (n=10) massifs. The Moa-Baracoa samples were grouped by these authors into three categories: H - harzburgites (n=7), D - dunites (n=3), and DI - impregnated dunites (n=6). The Mayarí-Cristal samples were grouped as: HN - northern harzburgites (n=2), HS - southern harzburgites (n=4), and DS - southern dunites (n=4), corresponding to back-arc basin (BAB) and forearc settings, respectively, according to the aforementioned authors. Additionally, samples from the work of Butjosa *et al*. (2018) in Villa Clara (n=20) were used, classified as: Group A - abyssal and fracture zone serpentinized peridotites (n=10), and Group B - forearc serpentinites (n=10). All data used are on an anhydrous basis.

Using the Statistica for Windows 11.0 software, the following diagrams were generated: (i) a classification diagram for ultramafic rocks (Le Maitre *et al*., 2002), and (ii) bivariate plots of MgO/SiO_2 vs. Al_2O_3/SiO_2; FeO^T wt% vs. Al_2O_3 wt%; CaO wt% vs. Al_2O_3 wt%; and TiO_2 wt% vs. Al_2O_3 wt%. These diagrams plot the compositional fields for the RUMC and the Mariana forearc, as proposed by Butjosa *et al*. (2018). For simplicity, the abbreviation "wt%" (from the English "weight percent") is used to indicate weight percentage.

3. RESULTS

3.1. Petrography of the Ultramafic Rocks in the SW Sector of the Cajálbana Massif

These rocks are frequently serpentinized and weathered. Small-scale tectonic structures such as folds, boudins, and fractures are commonly observed (Figure 2).

Figure 2. Serpentinized and weathered ultramafic rocks, showing small-scale folds, boudins, and fractures (photographs by J. A. García Hernández).

The studied lithologies are harzburgites and, to a lesser extent, dunites, based on their mineralogical and chemical composition (Tables 1 and 2; Figure 3). The former are characterized by a modal composition consisting of olivine (68% - 79%), orthopyroxene-enstatite (10% - 20%), and clinopyroxene-augite (up to 4%). Opaque minerals are also present, including Cr-spinel (0.2% - 3%) and magnetite (0.5% - 9.5%). The presence of serpentine-group minerals (8% - 18%) is notable, with some samples reaching high values (30% and up to 83%; Table 1).

Table 1. Mineralogical composition of the ultramafic rocks in the SW sector of the Cajálbana massif

No.	**Rock**									**Serpentine**	**Magnetite**	**Chromite**
		Ol	**Opx**	**Cpx**	**Op**	**Chr**	**Srp**	**Cb**	**Chl**			
M4-1	Hzg	68	15	-	1	1	15	-	-	Lz in bands, Veins of Ctl, Bst in Opx	In veins with Srp	Altered and fractured
M4-2	Hzg	72	14	2	1,5	0,5	10	-	-	Srp in borders of Ol, Veins of Ctl	In veins and well defined disseminated grains	Altered and fractured small grains
M4-5	Hzg	69	15	2	-	2	12	-	-	Srp rimming Ol, in veins	In veins and rims of Ol and Px	Altered and fractured small grains
M5-1	Hzg	70	10	2	2	1	15	-	-	Lz in bands, Veins of Ctl	Irregular veins, veins and fractures in Px	Altered to Mag or ChrFe Inclusion in Opx
M5-2	Hzg	70	12	2	3	1	12	-	-	Veins of Srp in Cpx, Lz in bands	Abundant veins abundantes	Altered to Mag or ChrFe Inclusion in Ol
M5-4	Hzg serp	15	45	-	9	1	30	-	-	Ctl	Disseminated and in veins	Altered grains to Mag or ChrFe
M5-5	Hzg	68	20	2	1	1	8	-	-	Veins of Srp throughout the rock	Irregular veins	Altered to Mag or ChrFe

M5-6	Hzg	72	10	2	3	3	10	-	-	Veins of Srp, Lz in bands	Veins	Altered to Mag or ChrFe
M5-7	Hzg	74	12	-	3	1	10	-	-	Veins of Ctl cross-cutting Opx	Veins	Slightly altered grains
MC-2	Hzg	78	8	4	4,5	0,5	2	-	3	Lz y Spf	Around Ol and Px	Scattered grains
MC-3	Hzg	69	15	2	2	1	10	1	-	Lz, sometimes Ctl	Veins	Fractured and altered to Mag or ChrFe
MC-4	Hzg	75	8	2	3	2	10	-	-	Ctl	Veins	Altered to Mag o ChrFe
MC-5	Hzg	60	15	4	2,5	0,5	18	-	-	Lz and Veins of Ctl cross-cutting Opx	Scattered, fine-grained related to Srp	Anhedral grains, fractured, with altered edges
MC-6	Dnt serp	-	10	-	8	2	80	-	-	Ctl, Lz y bastita en Opx	Diseminada y en Veins	Edges altered to Mg or ChrFe
MC-7	Dnt serp	-	7	-	9,5	0,5	83	-	-	Lz, Ctl in Veins and bastite in Opx	Disseminated in veins	Altered to Mag or ChrFe, mainly in edges
MC-9	Hzg	71	14	2	1	1	11			Lz in bands, Veins of Ctl	Disseminated and in veins	Altered in edges to Mag or ChrFe
MC-10	Hzg	79	15	-	2	2	12	-	-	Ctl in Veins, Bastite in Opx	Veins and rimming Ol and Px	Very fractured and altered to Mag o ChrFe,
MC-11	Hzg	77	8	2	1	2	10	-	-	Srp in networks and veins	In edges of Ol and Px	Slightly altered anhedral grains
MC-12	Hzg	84	10	1	1,5	0,5	3	-	-	Bands of Lz. Very fine Veins of Ctl and bastite in Opx	Veins	Very Slightly altered
MC-13	Hzg	76	10	2	0,5	1,5	10	1	-	Networks of Lz in Ol, Ctl	Veins and disseminated grains	Slightly altered to Mag or ChrFe and inclusions in Px
MC-14	Dnt	85	5	-	0,5	2	0,5	-	-	Lz in bands, Ctl in Veins and bastite in Opx	Veins and disseminated grains	Slightly altered

Note: Mineral symbols according to Whitney and Evans (2010): Ol - olivine, Opx - orthopyroxene, Cpx - clinopyroxene, Op - opaque minerals, Chr - chromite, Srp - serpentine, Cb - carbonates, Chl - chlorite, ChrFe - ferrochromite, Hzg - harzburgite, Dnt - dunite.

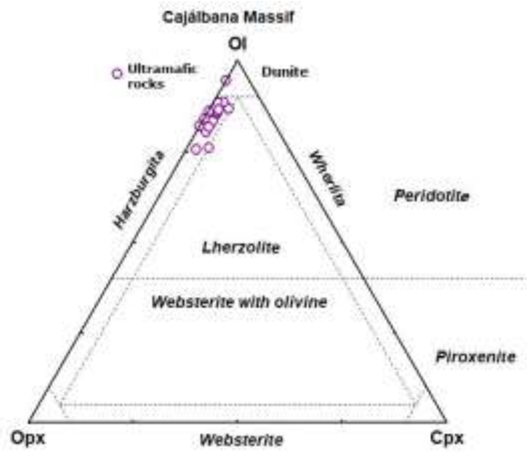

Figure 2. Classification diagram for the ultramafic rocks from the SW sector of the Cajálbana massif (after Le Maitre *et al*., 2002; see Table 2).

Olivine exhibits fractures filled with serpentine. Pyroxenes occur as porphyroclasts (Figure 4A) and display plastic deformations with kink band textures, undulatory extinction, and exsolution lamellae of clinopyroxene in orthopyroxene, alongside processes of serpentinization.

The dunites occur in two forms: (1) less altered varieties composed of olivine (~85%), ortho- and clinopyroxene (~5%), serpentine, and opaque minerals (Table 1); and (2) varieties with a high degree of serpentinization (up to 83%), where olivine is no longer preserved (Figure 4B), leaving only orthopyroxene porphyroclasts (7% - 10%) and opaque minerals. Both rock types contain subordinate minerals such as chlorite and carbonates (in thin veins) associated with the serpentine minerals (Figure 4).

3.2. Serpentinization and Opaque Minerals

Serpentinization is widespread, resulting from the alteration of olivine and pyroxene (Table 1). It is represented by bastite and various serpentine-group minerals (lizardite, chrysotile). Lizardita is very common in both dunite and harzburgite, typically occurring in a mesh texture (Figure 4D). Chrysotile is fibrous, growing perpendicular to vein boundaries; these veins cut irregularly across the rock (Figure 4E). Highly serpentinized samples (M5-4, MC-6, and MC-7) were not plotted on the Le Maitre *et al*. (2002) diagram.

The chromite-spinel observed in all lithologies appears as brown grains of variable size, ranging from 0.1 mm to 2 mm, often anhedral and fractured. It is commonly altered to Fe^{3+}-rich chromite-spinel (light brown color; Bach *et al*., 2006; Frost and Beard, 2007) or to magnetite, both along grain boundaries and within fractures (Figures 4F and 4G). The opaque minerals present in veins and as disseminated grains rimming olivine and pyroxene correspond to magnetite (formed from the alteration of these silicates).

Magnetite is more abundant in rocks with a higher degree of serpentinization (Figures 4C, 4D, 4H, and 4I).

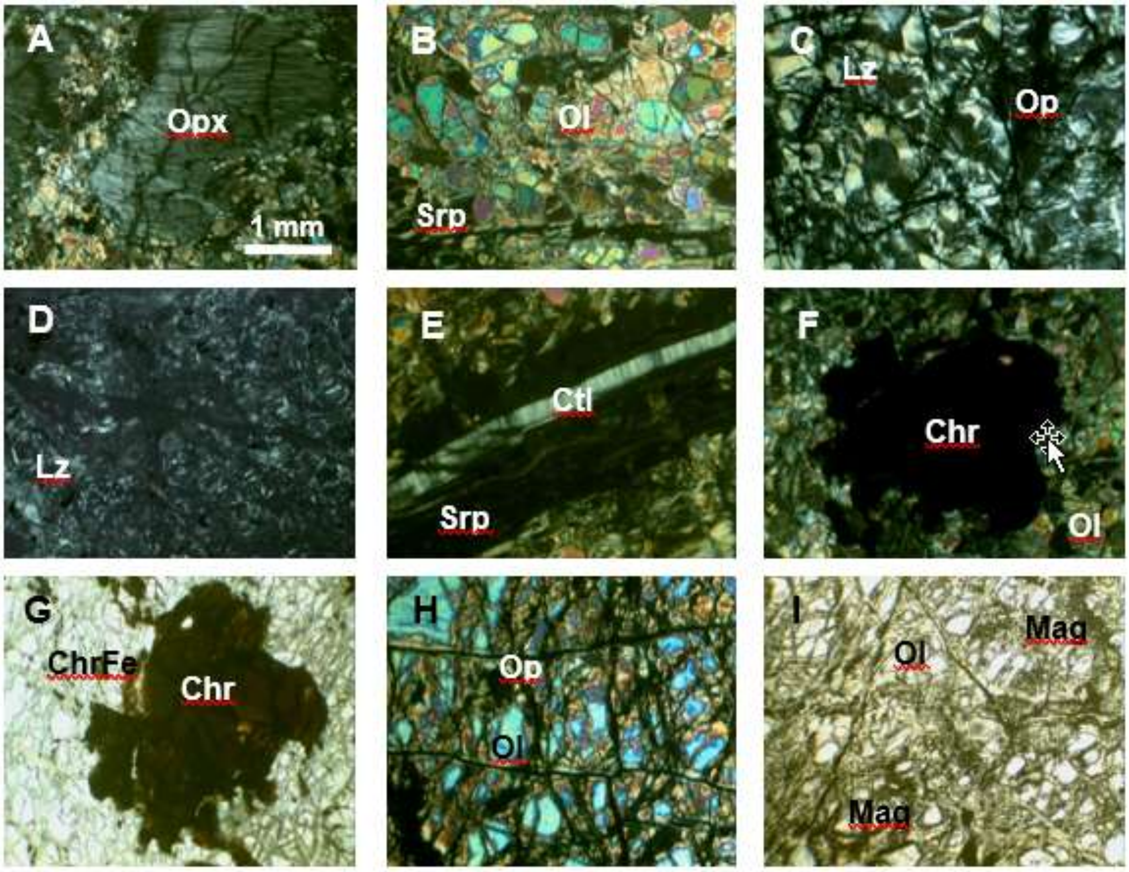

Figure 3. Photomicrographs of the ultramafic rocks. A: Fractured and bastitized orthopyroxene porphyroclast (M4-1). B: Olivine with serpentine rims in dunite (MC-14). C: Serpentinization process and opaque minerals in veinlets (MC-6). D: Lizardite exhibiting a ribbon-like habit (MC-7). E: Chrysotile vein in harzburgite (M5-7). F & G: Anhedral chromite grains in harzburgite (MC-11). H: Opaque mineral veinlets associated with olivine in harzburgite (MC-2). I: Modes of occurrence of opaque minerals: disseminated, in veins, and rimming olivine grains (MC-2). All images taken with a 4X objective and cross-polarized light (XPL), except G and I which are in plane-polarized light (PPL). The scale bar applies to all photomicrographs.

3.3. Geochemistry

The Loss on Ignition (LOI) values in the analyzed dunites and harzburgites (Figure 5, Table 2) range between 7 wt% and 15 wt%, indicating the degree of alteration due to serpentinization in these rocks (Deschamps *et al*., 2013).

Table 2. Major element composition of the ultramafic rocks in the SW sector of the Cajálbana Massif

Sample	**MC-2**	**MC-3**	**MC-4**	**MC-5**	**MC-6**	**MC-7**	**MC-9**	**MC-10**	**MC-11**	**MC-12**	**MC-13**	**MC-14**	**MC-15**
X	246170	246102	246049	245979	245880	245929	245376	245411	245545	245547	245408	245273	244931
Y	329686	329709	329722	329732	329752	329604	330176	330243	330241	330367	330439	330492	330715
Major Elements (wt %)													
SiO_2	40,40	40,63	40,55	40,92	38,75	38,38	39,74	38,24	39,65	40,54	39,79	40,01	39,58
TiO_2	0,03	0,03	0,04	0,03	0,01	0,02	0,03	0,01	0,02	0,02	0,02	0,02	0,02
Al_2O_3	1,77	1,67	2,12	2,17	1,19	1,45	2,09	1,05	1,48	1,44	1,42	1,60	1,45
Fe_2O_3	8,67	8,24	8,45	8,58	7,93	9,06	8,22	8,80	8,85	8,58	8,76	8,57	8,39
MnO	0,12	0,12	0,12	0,12	0,09	0,10	0,12	0,12	0,12	0,12	0,12	0,12	0,12
MgO	38,51	39,55	37,17	34,95	37,42	35,11	37,83	39,87	39,66	39,50	39,65	40,31	38,29
CaO	2,11	1,69	2,33	2,06	0,10	0,04	2,35	0,77	1,49	1,59	1,79	0,77	1,47
Na_2O	0,03	0,05	0,05	0,03	0,01	0,01	0,02	0,01	0,01	0,01	0,01	0,02	0,01
K_2O	0,01	0,01	0,01	0,01	0,01	0,01	0,01	0,01	0,01	0,01	0,01	0,01	0,01
P_2O_5	0,01	0,02	0,01	0,01	0,01	0,01	0,01	0,02	0,01	0,02	0,02	0,01	0,01
Cr_2O_3	0,326	0,353	0,362	0,405	0,427	0,406	0,453	0,256	0,379	0,340	0,337	0,358	0,457
PPI	7,60	7,30	8,40	10,40	13,80	15,00	8,80	10,50	8,00	7,50	7,70	7,90	9,90
TOTAL	99,59	99,66	99,61	99,69	99,75	99,60	99,67	99,66	99,68	99,67	99,63	99,70	99,71

The analysis revealed that the Ultramafic Rocks of the Cajálbana Massif (RUMC) maintain similar MgO/SiO_2 ratios and FeO^T wt% contents (ranging from 0.8 - 1.1 and 9 - 11, respectively; Figures 5a and 5b). In contrast, the Al_2O_3/SiO_2 ratios, and the Al_2O_3 wt% and TiO_2 wt% contents (ranging from 0.02 - 0.06, 1.17 - 2.43, and 0.01 - 0.04, respectively) are relatively variable (Figures 5a and 5d), while the CaO wt% contents are the most variable (ranging from 0.04 - 2.58; Figure 5c).

Furthermore, the studied rocks show a certain affinity with the Impregnated Dunites (DI) from Moa-Baracoa, the Northern Harzburgites (HN) from Mayarí-Cristal, and the Group A (GA) rocks from Villa Clara. Overall, this suite of rocks shares a geochemical identity with the abyssal field and the overlapping zones between this field and the forearc (Figures 5a-d).

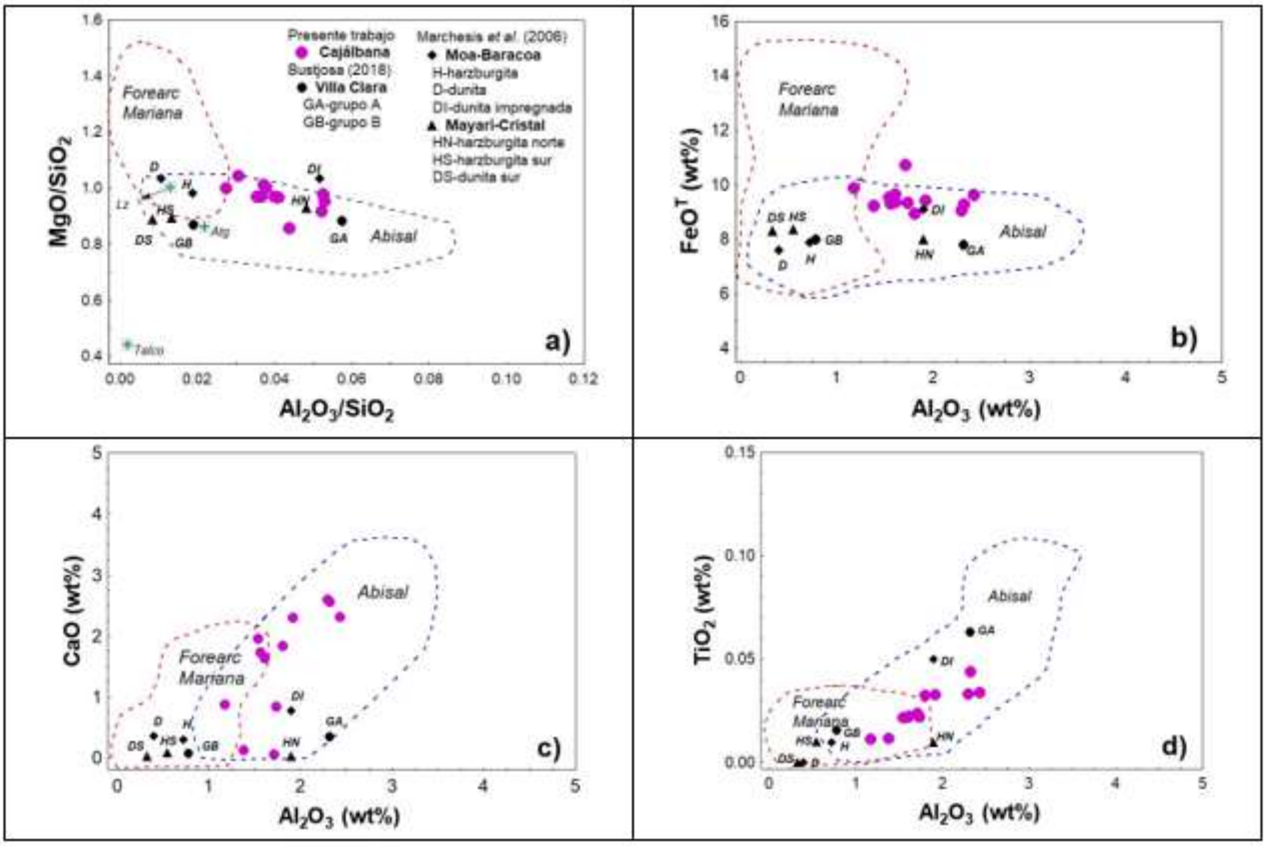

Figure 5. Compositional variation diagrams for the ultramafic rocks of the Cajálbana Massif (fields from Butjosa *et al*., 2018). a) MgO/SiO_2 vs. Al_2O_3/SiO_2; b) FeO^T wt% vs. Al_2O_3 wt%; c) CaO wt% vs. Al_2O_3 wt%; d) TiO_2 wt% vs. Al_2O_3 wt%. All oxides are on an anhydrous basis. Ultramafic rocks from various regions of Cuba are also plotted for comparison.

3. DISCUSSION

The analyzed rocks from the Ultramafic Rocks of the Cajálbana Massif (RUMC) are peridotites represented by harzburgite and, to a lesser extent, dunite, whereas other authors have described lherzolite and pyroxenite within this structure (Fonseca *et al*., 1984). Their mineral composition includes olivine, enstatite, augite, serpentine-group minerals, chromite-spinel, and magnetite. According to Coleman (1977), the serpentine-group minerals formed during hydration are lizardite, chrysotile, and antigorite. The lizardite and chrysotile observed in the RUMC represent low-temperature minerals (~350°C; Hekinian, 1982). Also related to serpentinization is the precipitation of iron-rich minerals (Fe^{3+}-rich chromite-spinel and magnetite); thus, under conditions of low SiO_2 content, magnetite can precipitate (Bach *et al*., 2006; Frost and Beard, 2007). Serpentinization (hydrothermal alteration) produces optical zoning in primary chromite-spinel. Generally, the chromite-spinel cores are surrounded by Fe^{3+}-rich chromite-spinel, which is typically found at grain boundaries and within fractures (Figure 4G). Occasionally, magnetite rims develop, surrounding the cores and/or the rims of Fe^{3+}-rich chromite-spinel.

Based on these results, two mineralization stages are proposed during the tectono-magmatic evolution of the RUMC (Table 1, Figure 4). The mineralogical sequence (Figure 6) shows that Stage 1 corresponds to the magmatic process, involving the formation of olivine, pyroxenes (enstatite and augite), and primary chromite-spinel. The Stage 2 minerals were generated by the infiltration of hydrothermal fluids linked to rifting and obduction processes: lizardite, chrysotile, and bastite; in addition to Fe^{3+}-rich chromite-spinel and magnetite rimming the primary chromite-spinel (Gervilla *et al*., 2012), occurring as disseminated grains and rims around olivine and pyroxenes (Figure 4I).

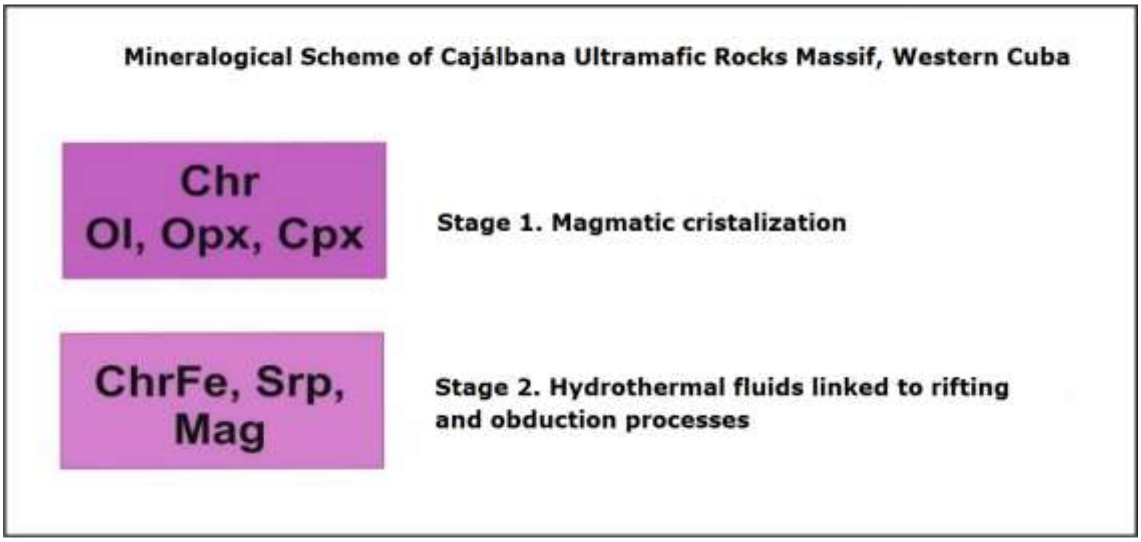

Figure 6. Mineral paragenesis sequence for the Ultramafic Rocks of the Cajálbana Massif (RUMC), based on the results from Table 1 (see abbreviations for mineral symbols).

As previously indicated, the RUMC exhibit an affinity for the abyssal type and the overlapping zones between this field and the forearc, closely approximating the fields occupied by the Impregnated Dunites (DI) from Moa-Baracoa, the Northern Harzburgites (HN) from Mayarí-Cristal, and the Group A (GA) rocks from Villa Clara (Marchesi *et al*., 2006; Butjosa *et al*., 2018). This dual geochemical behavior was also identified by Proenza *et al*. (2019) based on Rare Earth Element (REE) analysis of this massif. Among the samples analyzed by Proenza *et al*. (2019), four correspond to the abyssal type and two to SSZ peridotites.

Other authors, based on geochemical studies of basalts from the Encrucijada Formation (Figures 1b and 1c), assign a Back-Arc Basin (BAB) setting (Cruz-

Gámez, 1993; Cruz-Gámez and Méndez, 1997) and a MOR-Backarc setting (Llanes-Castro and Furnes, 2021) to this complex. This suggests that the affinity of the RUMC with the ancient proto-Caribbean crust or the Caribbean plate crust is not entirely clear.

A dual geochemical affinity has been documented in the Northern Ophiolitic Belt (NOB) of Cuban territory, encompassing both subduction-related settings (forearc, BAB) and ocean floor settings (abyssal-MOR). The former predominantly characterizes the eastern massifs (Camagüey, Mayarí, and Moa-Baracoa; Proenza *et al*., 1999 a,b; Marchesi *et al*., 2006; Henares et al., 2010), while a duality of settings is observed in different sections of the Villa Clara and Habana-Matanzas massifs (Butjosa *et al*., 2018; Llanes-Castro *et al*., 2015; Iturralde-Vinent *et al*., 2016). Therefore, a similar duality could also be present in the ophiolites of the RUMC.

5. CONCLUSIONS

- Two principal stages of mineral formation are distinguished during the magmatic process and subsequent serpentinization of the harzburgites and dunites of the RUMC: (1) Formation of olivine, enstatite, augite, and primary chromite-spinel, and (2) Formation of lizardite, chrysotile, Fe^{3+}-rich chromite-spinel, and magnetite. The latter stage is linked to the infiltration of hydrothermal fluids associated with rifting and obduction processes.

- The RUMC exhibit compositional variations within the range of ultramafic rocks from abyssal settings and the overlapping zones between this environment and the forearc. This is determined by the variation in the Al_2O_3/SiO_2 ratio and the weight percentages of Al_2O_3, TiO_2, and CaO (0.02 - 0.06, 1.17 - 2.43, 0.01 - 0.04, and 0.04 - 2.58, respectively). This geochemical behavior is also manifested in rock assemblages from other constituents of the Northern Ophiolitic Belt (NOB).

6. REFERENCIAS

Bach, W., Paulick, H., Garrido, C. J., Ildefonse, B., Meurer, W. P. & Humphris, S.E. (2006). Unraveling the sequence of serpentinization reactions: petrography, mineral chemistry, and petrophysics of serpentinites from mar 15°N (Odp Leg 209, Site 1274). *Geophysical Research Letters*, *14*, 1- 4. https://Doi.Org/10.1029/2006gl025681

Butjosa Molines, L. (2018). The petrogenesis of the ophiolitic mélange of Central Cuba: Origin and evolution of oceanic litosphere from abyssal to subduction and suprasubduction zone settings. [Tesis De Doctorado, Universidad De Barcelona]. http://Hdl.Handle.Net/2445/122449

Butjosa, L., Cambeses, A., Proenza, J. A., Agostini, S., Iturralde-Vinent, M., Bernal-Rodríguez, L. & García-Casco, A. (2023). Relict abyssal mantle in a Caribbean Forearc Ophiolite (Villa Clara, Central Cuba): Petrogenetic and geodynamic implications. *International Geology Review*, *65*, 196-227. https://Doi.Org/10.1080/00206814.2023.2179229

Cruz-Gámez, E. M. (1993). Papel del vulcanismo básico en la formación de los yacimientos cupro-piríticos de la zona estructuro–facial Bahía Honda, Pinar del Río. [Tesis De Doctorado, Universidad De Pinar Del Río].

Cruz-Gámez, E. M. & Simón, A. (1997). Principales rasgos del complejo de basaltos en la región de Bahía Honda. *Minería y Geología*, *14*(3), 25-31.

Coleman, R. G. (1971). Petrologic and geophysical nature of serpentinites. *Geological Society of America*, 82(4), 897-917.

Deschamps, F., Godard M., Guillot, S. & Hattori, K. (2013). Geochemistry of Subduction Zone Serpentinites: A Review. *Lithos*, 178, 96-127.

Dilek, Y. & Furnes, H. (2011). Ophiolite genesis and global tectonics: geochemical and tectonic fingerprinting of ancient oceanic lithosphere. *Bulletin*, *123*(3-4), 387- 411. https://Doi.Org/10.1130/B30446.1

Fonseca, E., Zelepuguin, M. & Heredia, M. (1984). Particularidades de la estructura de la asociación ofiolítica en Cuba. *Ciencias de la Tierra y del Espacio*, *9*, 31-46.

Frost, B. & Beard, J. S. (2007). On silica activity and serpentinization. *Journal of Petrology*, *48*, 1351-1368. https://Doi.Org/1351-1368.10.1093/Petrology/Egm0211

García-Casco, A., Pérez De Arce, C., Millán-Trujillo, G., Iturralde-Vinent, M., Fonseca, E., Torres-Roldán, R. L., Núñez-Cambra, K. & Morata, D. (2003). Metabasites from the northern serpentinite belt (Cuba) and a metamorphic perspective of the plate tectonic models for the caribbean region. Taller Del Proyecto Nº 433 Del Picg/Unesco "Tectónica De Placas En El Caribe". Geomin 2003, La Habana, Cuba.

García-Casco, A., Lázaro-Calisalvo, C., Rojas-Agramonte, Y., Kröner, A., Torres-Roldán, R. L., Núñez-Cambra, K., Neubauer, F., Millán-Trujillo, G. & Blanco-Quintero, I. F. (2008). Partial melting and counterclockwise P-T path of subducted oceanic crust (Sierra del Convento Mélange, Cuba). *Journal of Petrology*, *49*(1), 129-161. https://Doi.Org/10.1093/Petrology/Egm074

García-Casco, A., Iturralde-Vinent, M., & Pindell, J. (2008). Latest cretaceous collision/accretion between the Caribbean Plate and Caribeana: Origin of metamorphic terranes in the Greater Antilles. *International Geology Review*, *50*, 781-809. https://Doi.Org/10.2747/0020-6814.50.9.781

Gervilla, F., Proenza-Fernández, J. A., Frei, R., González-Jiménez, J. M., Garrido, C. J., Melgarejo, J. C., Meibom, A., Díaz-Martínez, R. & Lavaut-Copa, W. (2005). Distribution of platinum-group elements and Os isotopes in chromite ores from Mayarí-Baracoa ophiolitic belt (Eastern Cuba). *Contributions to Mineralogy and Petrology*, *150*, 589-607.

Gervilla, F., Padrón Navarta, J. A., Kerestedjian, T., Sergeeva, I., González Jiménez, J. M. & Fanlo, I. (2012). Formation of ferrian chromite in podiform chromitites from the Golyamo Kamenyane serpentinite. Eastern Rhodopes, Se Bulgaria: A two-stage process. *Contributions to Mineralogy and Petrology*, *164*, 643-657.

Hekinian, R. (1982). Petrology of the ocean floor. An Edition of petrology of the ocean floor, *Elsevier Oceanography Series* 33.

Henares, S., González-Jiménez, J. M., Gervilla, F., Proenza, J. A., Chang, A. & González-Pontón, R. B. (2010). Las cromititas del complejo ofiolítico de Camagüey, Cuba: Un ejemplo de cromitas ricas en Al. *Boletín Sociedad Geológica Mexicana*, 62 (1), 173-185.

Kravchenko, G. & Vázquez Santana, O. (1985). Estructura y perspectivas cromíferas de algunas regiones de los macizos ultrabasíticos de Cuba. *Ciencias de La Tierra y del Espacio*, *10*, 37-55.

Iturralde-Vinent, M. (1990). Las ofiolitas en la constitución geológica de Cuba. *Ciencias de La Tierra y del Espacio*, 17, 8-26.

Iturralde-Vinent, M. (1996). Geología de las ofiolitas de Cuba, En: Iturralde-Vinent, M.A. (Ed), *Ofiolitas y arcos volcánicos de Cuba*. International Geological Correlation Program Project *364*, 179–189.

Iturralde-Vinent, M. A., Garcia-Casco, A., Rojas-Agramonte, Y., Proenza, J. A., Murphy, J. B., & Stern, R. J. (2016). The geology of Cuba: A brief overview and synthesis, *Gsa Today*, *26*, 4–10. https://Doi.Org/10.1130/Gsatg296a.1

Llanes-Castro, A. I., Proenza J. A., Zaccarini, F., Garuti, G. & Pacheco Sarlabous, M. S. (2015). Al- and Cr-rich chromitites from the eastern Havana-Matanzas ophiolites (Western Cuba). *American Mineralogist*, *94*, 1459–1467. https://Doi.Org/10.18814/Epiugs/2015/V38i4/82429

Llanes-Castro, A. I. & Furnes, H. (2021). *Geochemical fingerprinting of ancient oceanic basalts: classification of the cuban ophiolites*. Springer.

Le Maitre, R. W., Streckeisen, A., Zanettin, B., Le Bas, M. J., Bonin, B., Bateman, P., Bellieni, G., Dudek, A., Efremova, S., Keller, J., Lameyre, J., Sabine, P. A., Schmid, R., Sorensen, H. & Woolley, A. R. (2002). *Igneous rocks. A classification and glossary of terms.* Ed. Cambridge University Press, Cambridge.

Marchesi, C., Garrido, C. J., Godard, M., Proenza-Fernández, J. A., Gervilla, F. & Blanco-Moreno, J. A. (2006). Petrogenesis of highly depleted peridotites and gabbroic rocks from the Mayarí-Baracoa ophiolitic belts (Eastern Cuba).

Contributions To Mineralogy And Petrology, *151*, 717-736. https://Doi.Org/10.1007/S00410-006-0089-0

Prieto, C. M., Llanes Castro, A. I., Mayeta, R., Ramos, R. & García- Hernández, J. A. (2017). Caracterización mineralógico textural del sector sur-oeste del macizo Cajálbana, La Palma, Pinar del Río. *Infomin*, 9(2), 10-24.

Proenza, J., Gervilla, F. & Melgarejo, J. C. (1999 a). La Moho Transition Zone en el macizo ofiolítico Moa-Baracoa (Cuba): Un ejemplo de interacción magma/peridotita. *Revista de la Sociedad Geológica de España*, *12*(3-4), 309-327.

Proenza, J., Gervilla, F., Melgarejo, J. C., Bodinier J. L. (1999 b). Al-rich and Cr-rich chromitites from the Mayarí-Baracoa ophiolitic belt (Eastern Cuba): Consequence of interaction between volatile-rich melts and peridotites in suprasubduction mantle. *Economic Geology*, *94*, 547-566.

Proenza, J. A., García-Casco, A., Rojas-Agramonte, Y., Iturralde-Vinent, M. A., Marchesi, C., Lázaro, C., Blanco-Quintero, I. F., Butjosa, L., Cárdenas-Párraga, J., Gervilla, N. F., Farré De Pablo, J., & Llanes-Castro, A. I. (2019). Age and petrogenesis of cuban ophiolites. VIII Convención de Ciencias de la Tierra. La Habana, Cuba.

Whitney, D. & Evans, B. W. (2010). Abbreviations for names of rock-forming minerals. *American Mineralogist*, *95*, 185-187.

Additional Information

Conflict of Interest

The authors declare no conflicts of interest.

Authors´ Contributions

MEGC, EMCG: Data processing, microscopic description, creation and interpretation of graphs, manuscript preparation, review and editing, approval of the final version. RRP: Fieldwork, sample collection, approval of the final version.

ORCID

MEGC: https://orcid.org/0000-0002-0406-2773
EMCG: https://orcid.org/0000-0001-8887-7277
RRP: https://orcid.org/0009-0001-6475-2848

Received: 04/10/2024
Accepted: 25/11/2025